Aerosol Optical Characteristics in the Yellow Sand Events Observed in May, 1982 at Nagasaki-Part II Models

By Teruyuki Nakajima, Masayuki Tanaka, Maki Yamano[1]

and

Masataka Shiobara[2]

Upper Atmosphere Research Laboratory, Tohoku University, Sendai 980, Japan

Kimio Arao

Faculty of Education, Nagasaki University, Nagasaki 852, Japan

and

Yuji Nakanishi[3]

EKO Instruments Co., 1-21-8, Hatagaya, Shibuya-ku, Tokyo 151, Japan
(Manuscript received 2 November 1988, in revised form 14 February 1989)

Abstract

Phase functions of yellow sand particles were measured by a polar nephelometer during 24 April–11 May, 1982 at Nagasaki, Japan. They suggested a strong nonsphericity of the particles, which can be reconstructed by the semi-empirical theory of Pollack and Cuzzi or by Mie particles with large fictitious absorption. Spectral extinction cross section, single scattering albedo, asymmetry factor and backscattering phase function were estimated using the volume spectra retrieved from data of several instruments including the polar nephelometer data. Volume loading of yellow sand particles at the observation site was estimated as 666 l/km^2 at the maximum stage of the yellow sand event of 4–6 May and 183 l/km^2 for the secondary maximum of 8 May. Using two estimates of the absorption index (0.01 and a model variable with wavelengths), these values show that solar radiative heating from 0.08 to 0.4°C/day can be expected in the atmosphere over considerably wide area in one yellow sand event.

1. Introduction

Studies of the radiative effect of aerosols have rested on the Mie scattering theory assuming homogeneous spherical dielectrics (Mie particles). As for a strong perturbation of the radiation regime by dust storms, however, such an assumption seems to be too simplified, because dust particles have irregular shapes (Tanaka *et al.*, 1987; Okada *et al.*, 1987) and are large enough to affect the light scattering property. Welch *et al.* (1981) showed that it is possible to overestimate the particle concentration by several tens of percent if we neglect the nonsphericity in the analysis of flux measurements. Otterman *et al.* (1982) suggested that their satellite remote sensing method overestimates the single scattering albedo if the nonsphericity of dust particles is neglected. In spite of such observations, we prefer to use the Mie scattering theory because of its simplicity and uncertainty in how to describe the nonsphericity. Although there are many theories for calculating the light scattering properties of nonspherical particles (*e.g.*, Asano and Sato, 1980; Mugnai and Wiscombe, 1986), we must assign the exact shape of particles before applying those theories. Since we see almost infinite kinds of particle

[1]Present address: 2-9-10, Nagao, Tama-ku, Kawasaki 214, Japan.

[2]Present affiliation: Meteorological Research Institute, Tsukuba 305, Japan.

[3]Present affiliation: Stabilizer Co. Ltd., 2-22-23, Nishiōizumi, Nerima-ku, Tokyo 177, Japan.

shape in a microscope image, it is not an easy task to determine reasonable statistics for the particle shape. Therefore, it will be very useful to accumulate measurement data of phase functions in real conditions of dust storms. There has been little work in this direction. Especially there are no investigations of the phase function of yellow sand particles in the North-Eastern Asia to our knowledge .

The scattering property of each nonspherical particle depends on its shape as shown by a number of measurements of light scattering by nonspherical particles in laboratory conditions (*e.g.*, Holland and Gagne, 1970; Pinnick *et al.*, 1976; Chýlek *et al.*, 1977; Zerull, 1976; Schuerman *et al.*, 1981; Coletti, 1984). For example, the asymmetry factor can increase or decrease as compared with the equal-volume sphere, depending on the particle shape and size (Mugnai and Wiscombe, 1986). In spite of the variety of the scattering patterns for a variety of the particle shapes, there may be some possibility of describing its general features using a semi-empirical fitting as in Pollack and Cuzzi (1980). Basically the phase functions of nonspherical particles are less dependent on the scattering angle than that of Mie particles (Coletti, 1984). The degree of linear polarization also tends to become smaller than that of Mie particles.

In this paper we study *in situ* measurements of the phase function of yellow sand particles using a polar nephelometer for the yellow sand events of 1982 (Tanaka *et al.*, 1989). We describe some general features common in observed phase functions and try to fit the function using the semi-empirical theory of Pollack and Cuzzi (1980) or introducing a fictitious absorption into Mie particles. As the result of such study and the volume spectra retrieved from several instruments, we will calculate the spectra of the extinction cross section, moments of the phase function and the backscattering phase function.

2. Measurements

As described in Part I of our papers (Tanaka *et al.*, 1989) we carried out measurements of solar radiation and aerosols during the period from 22 April to 12 May, 1982. We had two yellow sand events at Nagasaki, Japan during the period. We have divided the observation period into the maximum stage of the yellow sand event of 4–6 May, the secondary yellow sand event of 8 May, and the normal condition preceding and following the events. The strong enhancement of the forward light scattering was observed in the yellow sand events showing dominance of large sand particles of several microns. In the same period, we carried out measurements of the phase function using a polar nephelometer.

The polar nephelometer was newly designed for the purpose of field work as shown in Fig. 1. Linearly polarized light from a He-Ne laser (NEC/GLG-5700, the output light power of 25 mW at the wavelength $\lambda = 0.6328$ μm) is guided into a chamber through two mirrors ($M1$ and $M2$), Glan-Thompson prism ($P1$) and a polarizer ($P2$) which is a sliding $\lambda/2$ retardation plate to rotate polarization axis of incident light by 90°. Scattered light is collected by an object lens ($P5$) of 110 mm in effective diameter through a rectangular prism ($P3$) and an analyzer ($P4$) on a horizontal turntable, and photon-counted by a photo-multiplier ($P.M.$: Hamamatsu Photonics, R649). The analyzer consists of two sliding linear polarizers parallel and perpendicular to the scattering plane. The field of view of the detector is limited by a shadowing screen (SS) as the rectangular prism rotates. By this optical alignment, we can measure scattered radiation at scattering angles from 7 to 170° within the scattering chamber of 1 m length. Changing the polarization state of the incident and scattered radiations by the polarizer and the analyzer, we can get the elements P_1, P_2, D_1 and D_2 of the phase matrix of air mass using following equation:

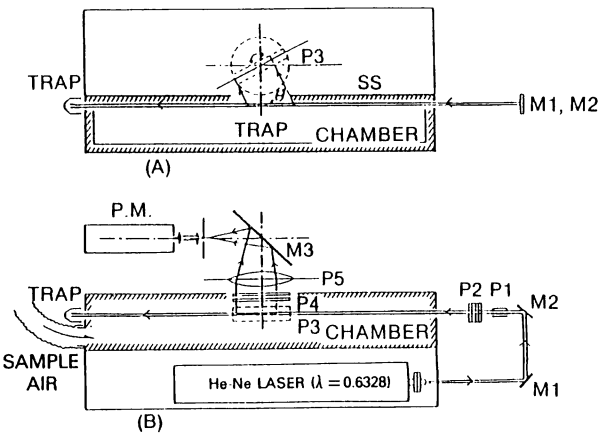

Fig. 1. Optical design of the polar nephelometer.

$$\begin{bmatrix} I_r \\ I_l \end{bmatrix} = \frac{s}{R^2} \begin{bmatrix} P_1 & D_1 \\ D_2 & P_2 \end{bmatrix} \begin{bmatrix} I_{or} \\ I_{ol} \end{bmatrix} \quad (1)$$

where (I_{0r}, I_{0l}) and (I_r, I_l) denote respectively incident and scattered radiations polarized perpendicularly and parallell to the scattering plane; s and R are the scattering cross section and distance between the scatterer and the detector. We observed the phase matrix at scattering angles of $\Theta = 7, 10, 15, 20(10)160, 165$, and 170°. Calibration of the light intensity was done using pure N_2 gas (Takamura and Tanaka, 1978). Measured phase functions were analyzed after subtracting the air molecule scattering, to retrieve the size distribution and refractive index of aerosols by the inversion-library method of Tanaka *et al.* (1982). The po-

lar nephelometer was set at the top of a building of Nagasaki University as well as other instruments described in Tanaka *et al.* (1989). For the nephelometer, the air was sampled with a rate of 70 *l*/min through an elephant tube of 50 mm diameter and 5 m long.

3. Light scattering property of the yellow sand particles

Figure 2 shows typical examples of the observed unnormalized phase functions, *i.e.*, sP_1 by circles and sP_2 by triangles, for aerosols near the ground surface in the normal condition (left panel) and the yellow sand event (right panel), respectively. We also show the linear polarization ratio and depolarization ratios defined as follows:

$$DP = (P_1 - P_2)/(P_1 - P_2) \tag{2}$$

$$DV = D_1/P_1 \text{ and } DH = D_2/P_2 \tag{3}$$

By lines in Fig. 2 we show unnormalized phase functions reconstructed by the method of Tanaka *et al.* (1982) assuming Mie scattering. In Fig. 2 we also listed the retrieved values of the refractive index (m), scattering cross section (s in cm^{-1}), single scattering albedo (ω), backscattering phase function (P_b) which is the value of the normalized phase functions at $\Theta = 180°$, and relative root mean square deviation (rmsd) between theoretical and measured values (σ).

In the normal condition, the shape of the phase function and the associated refractive index were very similar to those of other measurements (Tanaka *et al.*, 1983). In the yellow sand events, however, we find a significant enhancement of the forward scattering caused by large particles, which was also observed in the solar aureole measurements (Tanaka *et al.*, 1989). In spite of this large forward peak, we can find no enhanced backward scattering, which is expected for large spherical particles with small absorption index as seen later in Fig.7. The backscattering phase function (P_b) took a value of 0.0211 for yellow sand particles as small as 0.0218 for the normal condition. The inversion-library method chose $1.70 - 0.08i$ as the optimum value of the refractive index in the case of the yellow sand events. This value of the refractive index is very large for both of its real and imaginary parts as compared with a realistic value around $1.55 - 0.005i$ for Saharan dust particles. It is considered that this unsuccessful estimation was caused by nonsphericity of the particles rather than by difference of the chemical composition of yellow sand particles from that of Saharan dust particles. Values of the depolarization ratio (DV and DH) reached 50 % as shown in Fig. 2 supporting this expectation. Depression of backscattering and large depolarization of light scattering by nonspherical particles have been reported by many

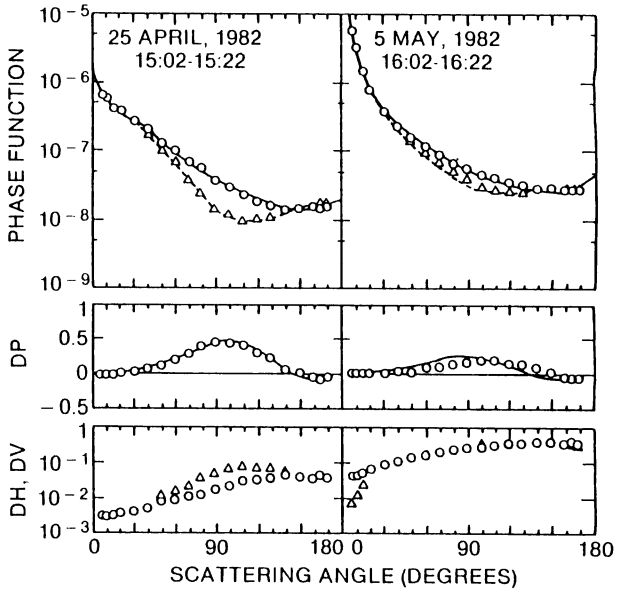

Fig. 2. Phase functions (○ and △), the degree of the linear polarization ratio (DP) and the depolarization ratios (DH, DV) on 25 April and 5 May, 1982. Lines show the reconstructed values using Mie theory with parameters: $m = 1.55 - 0.03i$, $s = 9.57 \times 10^{-7}$ cm^{-1}, $\omega = 0.828$, $P_b = 0.0218$ and $\sigma = 0.056$ for 25 April; $m = 1.70 - 0.08i$, $\sigma = 2.08 \times 10^{-6}$ cm^{-1}, $\omega = 0.602$, $Pb = 0.0211$ and $\sigma = 0.087$ for 5 May.

investigators from measurements and theories. In spite of the evidence of nonsphericity notable in the observed phase functions, the reconstructed phase functions of Mie particles with large fictitious absorption follow remarkably well observed phase functions including the linear polarization ratio (DP) as shown by lines in Fig.2. The relative rmsd (σ) between the observed and reconstructed phase functions was as small as 8.7 % in this example. Such similarity between nonsphericity and absorption in the phase function was also pointed out by Grams *et al.* (1974) and Pinnick *et al.* (1976).

Figure 3 shows the time series of the moments g_1, g_2 and g_4 of the Legendre expansion of the phase function:

$$P(x) = [P_1(x) + P_2(x) + D_1(x) + D_2(x)]/2 = \frac{1}{4\pi}\sum_n (2n+1) g_n P_n(x) \tag{4}$$

where $x = \cos\Theta$. The ratio of the total depolarized cross section D_S to the total scattering cross section s is given by

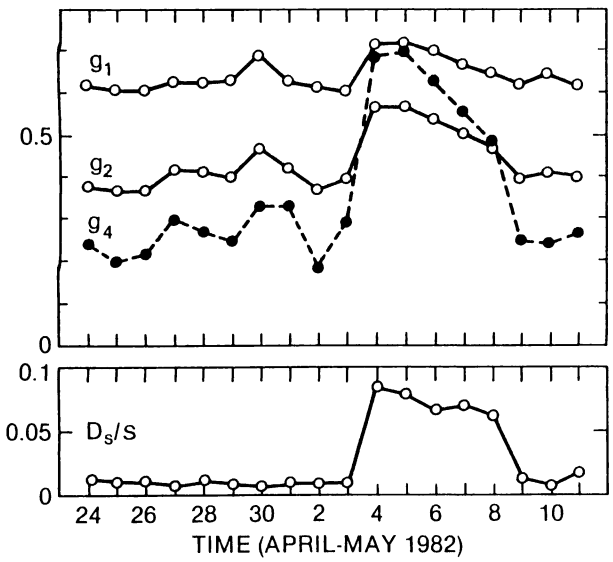

Fig. 3. Time series of moments of the phase function (g_1, g_2, g_4) and the total depolarization ratio (D_s / s).

$$D_s/s = \frac{1}{2}\int_{-1}^{1}[D_1(x) + D_2(x)]dx \qquad (5)$$

In the normal condition, this ratio took values as small as 1 %, so that Mie particles will be a good approximation for aerosols in the normal condition. In the yellow sand events, on the other hand, g_4 increased about 3 times that of the normal condition and the depolarized cross section reached about 10 % of the total scattering cross section showing nonsphericity of particles. Although the depolarization ratios (DV and DH) differed from each other and depended on scattering angles, the elements D_1 and D_2 took similar values almost independent of scatte ring angles through the observation period. This means that orientations of aerosols were distributed randomly through the period regardless of conditions.

Mean values of g_1 and g_2 were respectively 0.631 ± 0.320 and 0.407 ± 0.218 for the normal condition, 0.713 ± 0.157 and 0.563 ± 0.128 for the period of 4 - 6 May, and 0.651 ± 0.026 and 0.474 ± 0.027 for 8 May. Small rmsd values of these parameters in the yellow sand events show that the size distribution of yellow sand particles was relatively stable during one or two days as noted from the constancy of α shown in Fig. 7 of Part I. According to Nakajima *et al.* (1986),values of g_1 and g_2 in Sendai, Japan were relatively constant in autumn and were 0.615 and 0.391, respectively, indicating the air mass of Nagasaki in the normal condition was characterized by somewhat larger aerosols.

4. Modelling the aerosol optical scattering

Since yellow sand particles showed a strong nonsphericity as studied in the previous section, we must be careful to model the optical characteristics of the particles. In this section, we discuss the volume spectrum consistent with the interpretation of several instrumental results including the phase function data and try to obtain spectra of the optical characteristics by integrating the volume spectrum assuming a scattering theory of nonspherical particles.

(a) Model volume spectra

To see the variability of the retrieved volume spectra from various instruments, we show the averaged volume spectra in the normal (Fig. 4), the maximum stage of the yellow sand event condition during 4 - 6 May (Fig. 5), and the secondary stage of 8 May (Fig. 6). Since the OPC signal was calibrated using polystyrene particles having the refractive index of $1.60 - 0i$, correction of the refractive index from $1.60 - 0i$ to $1.50 - 0.01i$ has applied to the data in the normal condition. For transformation of the vertical coordinate of the columnar data (denoted as $A + O$), the scale height of the aerosol layer was assumed to be 5 km, 2.6 km and 5 km for these periods, respectively. Since yellow sand particles are sometimes multi-layered as reported by Shaw (1980) and Iwasaka *et al.* (1982), the scale height necessarily does not correspond to the mean height of the layers.

For the normal condition, the volume spectra from various methods agreed well with each other for $r \geq 0.8$ μm. For smaller particles, however, the columnar volume spectrum ($A + O$) did not show a peak around 0.2 μm corresponding to the accumulation mode for the surface data. We should note that the averaged columnar volume spectrum tended to become flat as a result of averaging multi-modal spectra having different peaks as shown in Figs. 9 and 10 of Part I. Peaks at different mode radii will be associated with aerosols of different origin.

For the yellow sand events (Figs. 5 and 6), the volume spectra from various methods agreed well in their general features. Inverted volume spectra from the nephelometer data with an abnormally large absorption ($1.70 - 0.08i$) also follow other profiles. For a more realistic refractive index such as $m = 1.55 - 0.005i$, we had an unrealistic volume spectrum different significantly from other profiles. Such unsuccessful retrievals due to nonsphericity (which would have an effect similar to assuming the wrong refractive index) were also pointed out by others (Shifrin and Gashko, 1974; Gorchakov *et al.*, 1976; Heintzenberg and Welch, 1982). Similarity between the nephelometer result and other profiles, therefore, show some similarity between effects of nonsphericity and absorption. As already shown in

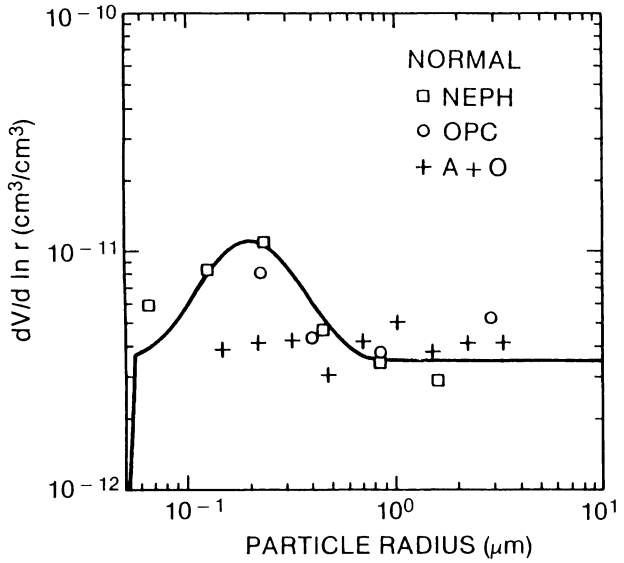

Fig. 4. Averaged volume spectra in the normal condition obtained by the nephelometer (NEPH), optical particle counter (OPC) and aureolemeter (A+O). The line shows the model NM.

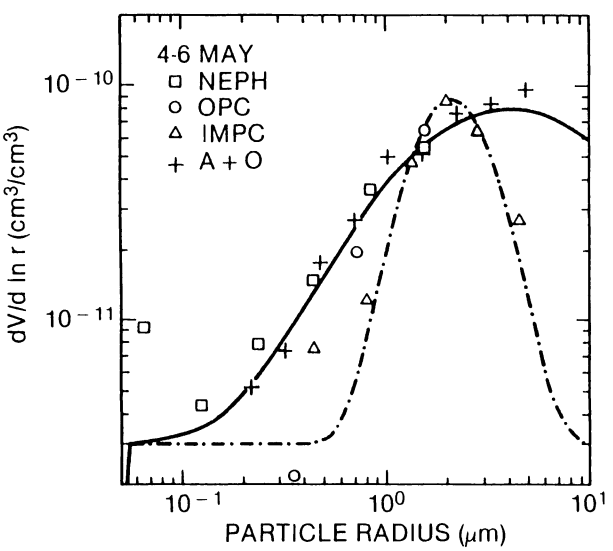

Fig. 5. Same as Fig. 4 but for 4–6 May. The result of Andersen sampler is shown by IMPC. The solid and dashed lines show the models YA and YC, respectively.

Part I, Figs. 4 – 6 show that the volume concentration of submicron particles in the yellow sand events was smaller than that in the normal condition.

In the detail of Figs. 5 and 6 we can see several discrepancies depending on instruments. The Andersen sampler result has a dispersion smaller than that of other profiles. The Andersen sampler measured less aerosol volume at a radius 4.5 μm than

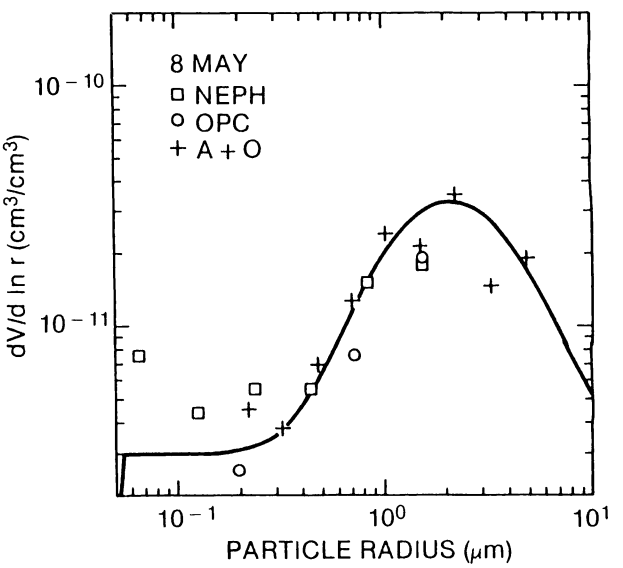

Fig. 6. Same as Fig. 4 but for 8 May. The solid line shows the model YB.

those of the maximum stage obtained by other instruments. The Andersen sampler data in Fig.5 is an integral of the volume spectrum during the sampling period of 4–6 May, so that large particles become less dominant by time averaging. If we fit this volume spectrum by a log-normal function, we have a dispersion smaller than that of other profiles in Fig.5. It is very difficult, however, to come to a sound conclusion because we could not have a good estimate for volume of submicron particles without sufficient sampling time. Another disagreement among the instruments in Figs. 5 – 6 is that at the maximum stage the amount of submicron particles from the nephelometer agreed well with the columnar spectrum, while the OPC result showed a smaller amount of submicron particles. We will discuss this disagreement later.

To model the observed volume spectra during the observation period, we fit the data to the following log-normal plus power law function:

$$dV/d\ln r = C_L \exp\{-[\ln(r/r_m)/\ln\delta]^2/2\} + C_J(r/r_m)^{4-p'} \quad (6)$$

with $p' = p$ for $r > r_m$ and $p' = 0$ for $r \leq r_m$. Lines in Figs. 4 – 6 are the fitted volume spectra with parameters shown in Table 1. We set as $p = 4$ and $r_0 = 0.1$ μm for all models, since this is not so sensitive to the results. For the yellow sand events we have three models, *i.e.*, models YA and YB for 4–6 May and 8 May to interpret the data of the aureolemeter, nephelometer and OPC, and the model YC for the data of Andersen sampler during 4–6 May. The model YC has a smaller dispersion than other two. For comparison, Table 2 lists values of r_m and δ obtained by fitting data from several studies of dust

Table 1. Parameters in Eq. (6) for model volume spectra (cm^3/cm^3) and the specific volume (cm^3/cm^3) in Eq. (13). A notation like 7.5–12 in the columns of C_L and C_J means 7.5×10^{-12}.

Type	$r_m(\mu m)$	δ	C_L	C_J	V_L	V_J	Scattering theory
NM	0.2	1.6	7.5–12	3.5–12	2.75	5.55	Mie
YA	4.0	3.0	7.7–11	3.0–12	1.74	5.55	$r = 1.1, X_0 = 7, G = 10$
YB	2.1	2.0	3.0–11	3.0–12	1.02	5.55	$r = 1.1, X_0 = 7, G = 7$
YC	2.1	1.5	8.7–11	3.0–12	1.18	5.55	$r = 1.1, X_0 = 7, G = 10$

Table 2. Mode radius (r_m) and dispersion (δ) of sand particle volume spectra.

r_m	δ	References
1.8	1.8	Shaw (1980) at Hawaii
1.3	1.6	Arao and Ishizaka (1986) at Japan
3.5	2.6	Carlson and Caverly (1977)
3.6	1.7	Kondratyev *et al.* (1981) at 0.5 – 1.5 km height
0.8	1.3	Tomasi *et al.* (1979) at Bologna
1.1	1.4	Tomasi *et al.* (1979) at Sestola
4.0	3.0	This study, Model YA
2.1	2.0	This study, Model YB
2.1	1.5	This study, Model YC

storms. These values show that wide variation in the volume spectrum is possible, depending on the history of aerosols, with some positive correlation between r_m and δ. As an average of the listed values, (r_m, δ) are (1.5, 1.5) for moderate dust storms and (3.5, 2.5) for heavy dust storms or at sites near the source.

Figure 7 shows the mean observed and the best fit total phase function, $s(P_1+P_2)/2$, at $\lambda = 0.6328\ \mu m$ for the periods of 4 – 6 May and 8 May. In the figure we have determined the coefficients C_L and C_J by two linear regressions: one is assuming Mie particles with $m = 1.70 - 0.08i$ (dashed line) and the other is assuming nonspherical particles expressed by the semi-empirical theory of Pollack and Cuzzi (solid line). For the latter, the semi-empirical phase function is described by parameters of x_0, G and r defined in the original paper. After many regressions for various sets of r, x_0 and G, we were able to determine the optimum values of (x_0, G) as (7, 10) for the period 4 – 6 May and (7, 7) for 8 May. Following the original paper we assume $r = 1.1$, since the fitting depends weakly on the value of r, which is the ratio of the surface area of the particle to that of the sphere of the equivalent volume. Morphological analysis of scanning electron microscope images of yellow sand particles showed that the distribution of the ratio of the minor radius to the major one had a mode around 0.6, which is equivalent to $r = 1.03$. Okada *et al.* (1987) also got a similar value. Larger values of x_0 and G compared with the cases studied by Pollack and Cuzzi show that the nonsphericity of

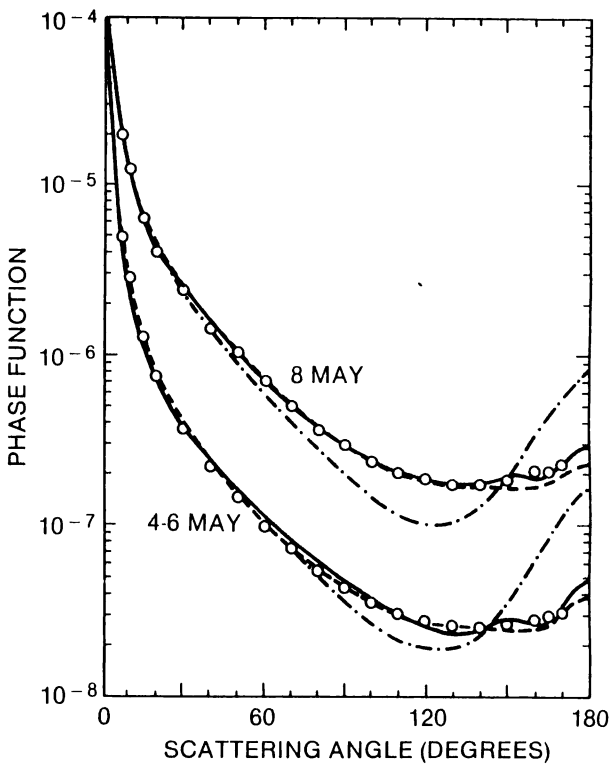

Fig. 7. Observed total phase functions of yellow sand particles for 4 – 6 and 8 May (O); Mie phase functions ($m = 1.55 - 0.005i$ —·—·—·—; $1.70 - 0.08i$ – – – –); the semi-empirical phase functions of nonspherical particles (—). The values for 8 May are shifted upward by one logarithmic scale.

Table 3. Extinction cross section ($\hat{e}$), single scattering albedo (ω), moments of the phase function (g_1, g_2) and backscattering phase function (P_b) in the normal condition (Table 3a) and the yellow sand event (Table 3b). Letters NM, YA, YB and YC in the model name show the volume spectrum; L and J indicate the modes of the volume spectrum; and A, T and V show the models of the refractive index (m). Units are cm^{-1} for $\hat{e}$; 1/1000 for ω, g_1 and g_2; 1/10000 for P_b.

(Table 3a)

λ	$\hat{e}$	ω	g_1	g_2	P_b	$\hat{e}$	ω	g_1	g_2	P_b
	NMJA	$m=$	1.53		$-0.024i$	NMJT	$m=$	1.55		$-0.005i$
0.35	2.60+5	829	665	461	235	2.64+5	949	636	440	426
0.40	2.30+5	827	660	458	240	2.33+5	949	633	437	430
0.50	1.86+5	823	656	455	246	1.88+5	949	629	434	433
0.70	1.34+5	818	652	452	251	1.34+5	948	625	432	437
1.00	9.44+4	812	650	450	253	9.40+4	948	623	430	439
1.50	6.29+4	807	648	447	255	6.22+4	948	621	427	442
2.00	4.71+4	804	646	443	256	4.62+4	949	619	424	441
2.50	3.76+4	801	645	441	257	3.68+4	949	618	423	442
3.00	3.12+4	800	643	439	259	3.05+4	949	617	421	443
	NMLA					NMLT				
0.35	1.37+5	881	711	503	172	1.43+5	972	679	480	308
0.40	1.26+5	886	702	480	153	1.31+5	974	674	461	255
0.50	1.01+5	889	678	436	138	1.06+5	975	657	421	201
0.70	6.19+4	881	621	357	153	6.39+4	974	609	349	182
1.00	3.04+4	852	529	272	229	3.08+4	967	525	269	238
1.50	1.13+4	778	393	191	401	1.03+4	948	396	191	399
2.00	5.25+3	681	291	150	564	4.27+3	918	295	151	559
2.50	2.92+3	572	219	130	695	2.08+3	875	222	130	689
3.00	1.86+3	466	168	118	796	1.14+3	820	171	119	791

yellow sand particles is more moderate and the size is larger than that of the cases in Pollack and Cuzzi. We can see that the value of x_0 of around 7 is reasonable as compared with the deviation of the asymmetry factor and backscattered fraction of Chebyshev particles from equal-volume spheres (Mugnai and Wiscombe, 1986).

The coefficients (C_L, C_J) are determined as (9.9×10^{-11}, 0) for 4 – 6 May and (3.3×10^{-11}, 4.0×10^{-12}) for 8 May, while for the absorbing Mie particle model they are determined as (1.1×10^{-10}, 6.7×10^{-12}) and (2.7×10^{-11}, 7.4×10^{-12}). It is found that the values of C_L are similar for both methods, while the values of C_J for absorbing Mie particles are much larger than those for nonspherical particles. This fact means that the effect of nonsphericity of yellow sand particles can be replaced by absorbing large Mie particles with an additional scattering by submicron particles (with increasing C_J). However, this analogy is not valid for the single scattering albedo since the absorbing Mie polydispersion has an extinction cross section larger than that of the nonspherical polydispersion for the same scattering cross section. This comparison between absorbing Mie particles and nonspherical particles is very useful in understanding the disagreement between the nephelometer and OPC results for submicron particles. If we reduce the volume of submicron particles of the nephelometer result as suggested by the preceding discussion, the result becomes rather similar to that of the OPC. This is consistent with an expectation that estimation of the volume spectrum by the OPC was good for particles smaller than 1 μm because the OPC signal is relatively insensitive to the nonsphericity and the assumed refractive index for submicron particles as explained just below. The OPC, RION KC-01, uses the mean scattering angle of $\Theta = 70°$ for light detection.

If we assume Mie particles with $m = 1.55 - 0.005i$ and the volume spectrum obtained by the nonspherical particles, then phase functions are given by dash-dotted lines in Fig. 7. Although these phase functions have a notable backscattering glory different from the observed one, the forward part at $\Theta \leq 70°$ is similar to other two phase functions. Therefore, it is found that the effect of the nonsphericity of the yellow sand particles is small in the forward part of the phase function, so that the volume spectra estimated from the OPC and the solar aureole data represent a good estimate for the yellow sand events.

(b) Model optical parameters

Several optical parameters of aerosols important in determining the solar radiative regime of the atmosphere are calculated as in Table 3 by using the model volume spectra derived in the preceding sub-

section. The table shows values for each mode (denoted by a letter L or J) of the volume spectrum models NM, YA, YB, and YC in Table 1. Since the listed values of extinction cross section ($\hat{e}$) are for $C_L = 1$ and $C_J = 1$, desired values of the extinction and scattering cross sections (e and s), single scattering albedo (ω), moments of the phase function (g_1 and g_2), and the backscattering phase function (P_b) for arbitrary values of C_L and C_J in Eq. (6) are obtained by following mixing rules:

$$e = C_L\hat{e}_L + C_J\hat{e}_J = e_L + e_J \tag{7}$$

$$s = C_L\hat{s}_L + C_J\hat{s}_J = s_L + s_J \tag{8}$$

$$\omega = s/e, \omega_L = s_L/e_L, \omega_J = s_J/e_J, \tag{9}$$

and

$$q = (s_L q_L + s_J q_J)/s \tag{10}$$

where $q = g_1$, g_2, or P_b. For the normal condition (Table 3a) we use the Mie theory with refractive indices of $1.55 - 0.005i$ (a transparent model labelled T in the model name) and $1.53 - 0.024i$ (an absorbing model labelled A) which is the average value obtained by the nephelometer. For the yellow sand event (Table 3b) we use the semi-empirical theory of Pollack and Cuzzi (1980) with parameters shown

(Table 3b)

λ	$\hat{e}$	ω	g_1	g_2	P_b	$\hat{e}$	ω	g_1	g_2	P_b	
	YAJA	$m =$	1.55		$-0.01i$	YAJV					$m = 1.55$
0.35	2.68+5	913	639	432	244	2.69+5	893	643	435	233	$-0.0130i$
0.40	2.37+5	912	635	429	249	2.36+5	926	633	427	256	$-0.0080i$
0.50	1.91+5	911	631	427	254	1.90+5	965	623	418	280	$-0.0033i$
0.70	1.37+5	909	628	424	258	1.36+5	978	617	414	289	$-0.0020i$
1.00	9.57+4	908	626	422	260	9.46+4	981	615	412	293	$-0.0017i$
1.50	6.35+4	907	624	419	262	6.26+4	980	614	410	295	$-0.0018i$
2.00	4.73+4	907	622	417	264	4.65+4	975	614	409	295	$-0.0024i$
2.50	3.76+4	906	621	415	266	3.71+4	953	616	410	288	$-0.0046i$
3.00	3.11+4	906	620	413	267	3.10+4	915	619	412	271	$-0.0090i$
	YALA					YALV					
0.35	2.29+4	760	768	639	148	2.27+4	729	781	659	141	
0.40	2.30+4	774	759	625	162	2.31+4	799	749	610	167	
0.50	2.34+4	796	744	602	185	2.37+4	902	712	552	203	
0.70	2.37+4	828	726	572	216	2.40+4	949	692	523	244	
1.00	2.36+4	858	709	544	242	2.39+4	966	681	506	280	
1.50	2.27+4	886	694	518	260	2.29+4	974	672	491	305	
2.00	2.13+4	902	685	500	266	2.14+4	972	668	482	311	
2.50	1.99+4	911	678	488	267	1.99+4	955	668	478	299	
3.00	1.84+4	918	673	478	267	1.84+4	925	671	476	273	
	YBLA					YBLV					
0.35	1.91+4	737	767	649	94	1.91+4	702	785	676	89	
0.40	1.94+4	754	754	630	112	1.94+4	783	741	610	115	
0.50	1.98+4	781	734	601	151	2.01+4	900	691	537	166	
0.70	2.07+4	821	709	565	221	2.10+4	950	667	506	251	
1.00	2.17+4	861	693	538	285	2.20+4	969	659	496	335	
1.50	2.25+4	897	684	516	313	2.27+4	977	660	491	375	
2.00	2.20+4	917	681	501	301	2.22+4	977	664	485	359	
2.50	2.09+4	928	678	487	282	2.10+4	964	668	479	318	
3.00	1.93+4	935	673	473	263	1.93+4	940	672	472	269	
	YCLA					YCLV					
0.35	9.26+3	692	823	722	38	9.24+3	655	842	754	38	
0.40	9.36+3	709	811	701	39	9.40+3	742	796	677	40	
0.50	9.54+3	739	790	665	42	9.69+3	879	740	584	44	
0.70	9.85+3	782	758	613	66	1.00+4	938	711	537	71	
1.00	1.02+4	823	721	564	171	1.03+4	960	684	507	194	
1.50	1.08+4	868	685	532	380	1.09+4	971	657	497	453	
2.00	1.19+4	903	682	529	424	1.20+4	973	661	509	509	
2.50	1.27+4	925	690	527	369	1.27+4	963	678	518	421	
3.00	1.29+4	938	695	517	302	1.29+4	944	693	516	309	

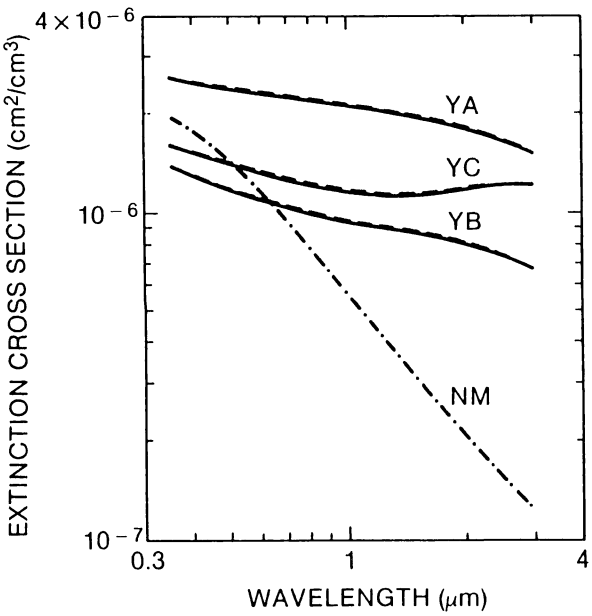

Fig. 8. Spectra of the extinction cross section (cm^{-1}) for models NMA (·····); YAV, YBV and YCV (- - - -); YAA, YBA and YCA (—).

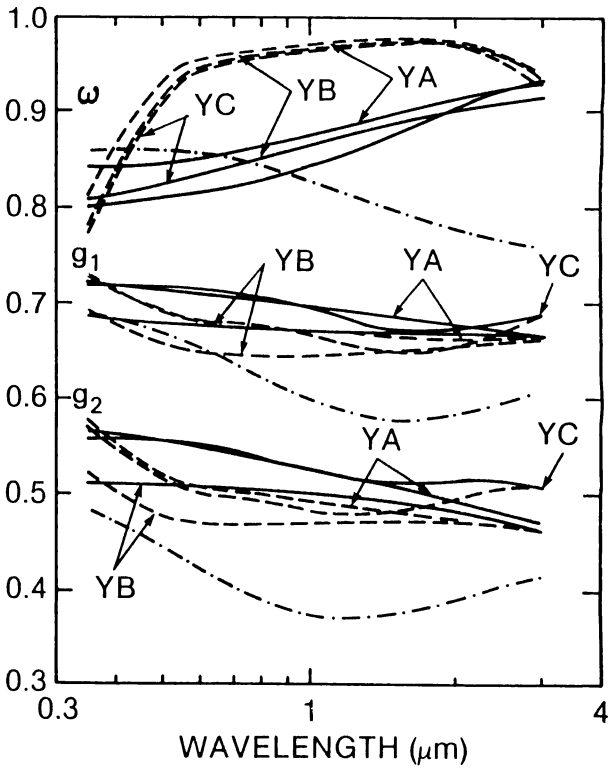

Fig. 9. Same as Fig. 8 but for the single scattering albedo (ω) and moments of the phase function (g_1 and g_2).

in Table 1 with two model spectra of the refractive index, *i.e.*, an absorbing model (labelled A) with $m = 1.55 - 0.01i$ independent of the wavelength; and a variable model (labelled V) with m of a function of wavelength which is determined after Carlson and Benjamin (1980). Since the results for $G = 7$ and $G = 10$ are nearly same for the mode J, we only show the models of $YAJA$ (that means the power law mode of the volume spectrum YA with the absorbing model of the refractive index) and $YAJV$ (same as $YAJA$ but with the variable refractive index model) for yellow sand particles.

Using the parameters in Tables 1 and 3, we calculated the spectra of the extinction cross section (Fig. 8), single scattering albedo and phase function moments g_1 and g_2 (Fig. 9), and the backscattering phase function P_b (Fig. 10). Figure 8 shows that the extinction cross section is relatively independent of the refractive index. In the yellow sand events, an enhancement of the extinction in the near infrared region (NIR) is significant, while the extinction for the visible light is comparable with that of the normal condition. In the visible region, the three models of yellow sand particles show a similar wavelength dependence, while the behavior of the model YC in the NIR is different from other two models.

The single scattering albedo of yellow sand particles ranges from 0.82 to 0.93 at $\lambda = 0.5$ μm depending on the assumed refractive index. Choice of the volume spectrum is relatively unimportant. Since there is large uncertainty in the reported values of the refractive index of soil derived particles (Carlson and Benjamin, 1980), evaluation of the spectral refractive index of yellow sand particles is desired as a future problem. The asymmetry factor (g_1) is relatively insensitive to the refractive index and volume spectrum. It is a weakly decreasing function of the wavelength for yellow sand particles and ranges 0.66 - 0.72 at $\lambda = 0.5$ μm which is slightly larger than that of the normal condition. Existence of the submicron accumulation mode in the normal condition increases significantly the moments in the visible wavelengths.

The magnitude of the backscattering phase function (P_b) depends strongly on the volume spectrum, refractive index, and wavelength with peaks around $\lambda = 1.5$ - 2 μm. Especially the model YC has a large backscattering around the peak. This is because of a selective enhancement of the backscattering cross section by the sharp peak of the volume spectrum. The large variety of P_b is serious obstacle to determining the backscattering ratio,

$$b = \frac{1}{\omega P_b} \tag{11}$$

which is necessary for the retrieval of the extinction cross section from the lidar signal. It ranges from 49 to 87 at $\lambda = 0.5$ μm and from 32 to 61 at $\lambda =$

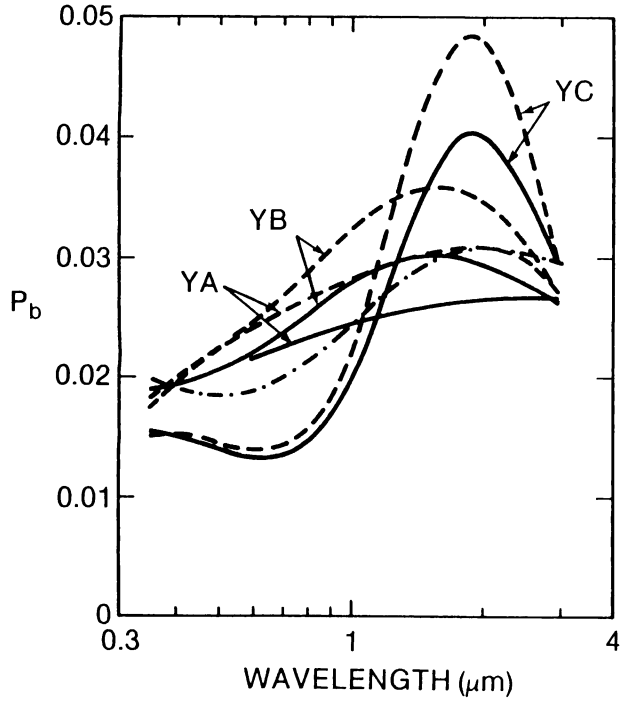

Fig. 10. Same as Fig. 8 but for the backscattering phase function.

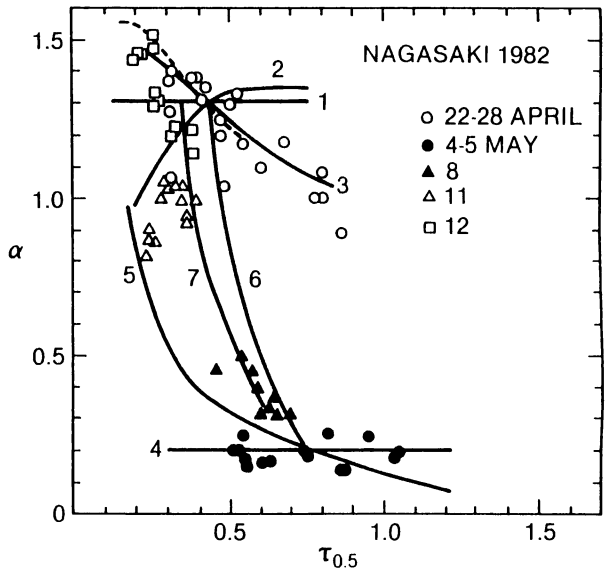

Fig. 11. Relationship between α and $\tau_{0.5}$ for various air masses in the observation period. Solid lines show the relationship given in Table 4. The dashed line shows the relationship in Fig. 7 of Kaufman and Fraser (1983).

1 μm. Being left with this large uncertainty, it is very interesting to measure the backward portion of the phase function at wavelengths from 1.5 to 2 μm. Also it is important to compile data of the volume spectrum, especially to know the typical dispersion of the volume spectrum for the yellow sand events.

5. Discussion

Using the results in the preceding sections, we can investigate furthermore the atmospheric turbidity condition during the observation period. Figure 11 shows the same plot as in Fig. 7 of Part I with model values of α and $\tau_{0.5}$ calculated by the mixing rules listed in Table 4 for two homogeneous polydispersions having the extinction cross sections (e_1 and e_2) and scale heights (H_1 and H_2):

$$\tau = H_1 e_1 + H_2 e_2 = \tau_1 + \tau_2 \qquad (12)$$

In Table 4, we distinguish the volume spectra (NM and YA) and its mode (log-normal mode as L and power law mode as J) attaching to quantities in Eq. (12).

In the normal condition, an increase of the mode L (line 2) causes an increase of α, while an increase of the mode J (line 3) causes a decrease of α. For the stage preceding the yellow sand events, the line 3 fits the trend of the observed data showing that the lognormal mode L was unchanged in the course of modification of the mode J. In this case the log-normal mode L would correspond to aerosols originating from surrounding urban type aerosol sources, while the power law mode J would correspond to the background aerosols. By a dashed line we show a relation for growing summer time aerosols absorbing water vapor with increasing humidity by Kaufman and Fraser (1983). The similarity of their line to the line 3 shows that the general trend between α and $\tau_{0.5}$ in the normal condition is caused by the humidity effect as already expected in Part I.

In the yellow sand event, an increase of the mode L causes a decreasing tendency of α. In the maximum stage of the yellow sand event, the observed data were more similar to the line 4, showing that the background mode J also changed correlating with the concentration of the sand particles. Lines 6 and 7 show a mixing process of two airmass of the normal condition and the yellow sand events with a mixing ratio k. The mixing lines follow well the observed data with slight overestimation of the optical thickness of 11 May. Some abrupt cleaning rather than the homogeneous mixing is expected in the decay stage of the yellow sand event.

From Eqs. (6), (7), and (12), we have the conversion factor from the optical thickness to the columnar total volume of aerosols as

$$V_c/\tau = [kV_L + (1-k)V_J]/[k\hat{e}_L + (1-k)\hat{e}_J] \qquad (13)$$

with

Table 4. Mixing rules for two homogeneous air masses as characterized by the extinction cross section (ϵ) and the scale height (H). The volume spectrum models and their modes are shown by labels attached to these quantities.

Type	Relation
1	$\tau = H_{NM}\epsilon_{NM}$ with $H_{NM} = H_{NML} = H_{NMJ}$.
2	$\tau = H_{NML}\epsilon_{NML} + H_{NMJ}\epsilon_{NMJ}$ with fixed H_{NMJ}.
3	same as Type 2 but with fixed H_{NML}.
4	$\tau = H_{YA}\epsilon_{YA}$ with $H_{YA} = H_{YAL} = H_{YAJ}$.
5	$\tau = H_{YAL}\epsilon_{YAL} + H_{YAJ}\epsilon_{YAJ}$ with fixed H_{YAJ}.
6	$\tau = k\tau_{YA} + (1-k)\tau_{NM}$.
7	$\tau = k\tau_{YB} + (1-k)\tau_{NM}$.

$$k = H_L C_L/(H_L C_L + H_J C_J) \quad (14)$$

and the specific volumes V_L and V_J for the modes L and J listed in Table 1 which are the aerosol volumes for $C_L = 1$ and $C_J = 1$, respectively. Equation (13) and Table 1 lead to $V_c/\tau = 284$, 634, 405, and 849 l/km^2 for the models NM, YA, YB, and YC, respectively, at $\lambda = 0.5$ μm for $H_L = H_J$. In this estimation, it is important to note that considerable extinction is caused by the mode J and the neglect of this mode of the volume spectrum leads to overestimation of yellow sand particles. In other words it is important to measure the concentration of submicron aerosols associated with the continental air mass along with that of large particles.

Values of the conversion factor show that yellow sand particles are large and not effective for scattering the solar radiation compared with the contribution of aerosols in the normal condition. Using the above conversion factor, we can evaluate the total columnar volume as 666 l/km^2 when the optical thickness of aerosols reaches 1.05 at the maximum stage, and as 183 l/km^2 when the optical thickness reaches 0.45 on 8 May . From these values it is found that the event of 4 – 6 May was more significant than the cases investigated by Arao and Ishizaka (1986) and Tomasi *et al.* (1979) where they reported values around 100 to 400 l/km^2, while these values are smaller than the value of 1000 l/km^2 for the average of Saharan dust of July 1974 at Sal (Carlson and Caverly, 1977). Since the corresponding average optical thickness at Sal was 0.74 at $\lambda = 0.5$ μm, the conversion factor for the Saharan dust was even larger than those of the present study due to the large size of the Saharan dust particles at Sal.

Since the single scattering albedo ranges from 0.85 to 0.97 at wavelengths around 1 m, energy convergence into the atmosphere due to aerosols in the yellow sand events was about $(1-\omega)\tau S = 3$ to 15 cal/day/cm^2, where S cal/day/cm^2 is a daily total of the effective solar insolation. This corresponds to a heating rate of about 0.04 to 0.2°C/day depending on the value of the single scattering albedo if the scale height of the aerosol layer is 3 km with the optical thickness of 0.1. These values are consistent with the detailed calculations of Carlson and Benjamin (1980). According to Arao and Ishizaka (1986), yellow sand particles of about 100 l/km^2 covered over Japan during about one day. The mean of the reported mass loading of Saharan dust at Italy is also about 100 l/km^2. These facts suggest that a heating rate about 0.08 to 0.4°C/day is expected over a considerably wide area in one yellow sand event. Since the aerosol loading reaches about ten times 100 l/km^2 at the maximum stage of the severe event, solar heating of several degrees is expected. Kondratyev *et al.* (1981) observed a heating rate as large as 9.6°C/day for a Saharan dust storm.

6. Conclusion

We measured the phase matrix for yellow sand particles in yellow sand events during 4–8 May at Nagasaki, Japan. Measured total phase functions can be fitted by the semi-empirical theory of Pollack and Cuzzi (1980) or by Mie particles with large fictitious absorption, showing some similarity between the light scattering by nonspherical particles and absorbing spheres. Large size and nonsphericity of yellow sand particles cause a distinct enhancement of forward scattering, suppression of backscattering, small linear polarization, and large depolarization as compared with the light scattering by aerosols in the normal condition. The asymmetry factor increased in the events as compared that in the normal condition.

We set model volume spectra for the normal condition and for the yellow sand events as in Table 1. Using the optical parameters tabulated in Table 3, which are calculated by the Mie theory and the semi-empirical theory of Pollack and Cuzzi, we estimated the spectra of the extinction cross section, single scattering, moments of total phase function, and the backscattering phase function as in Figs. 8 – 10. These figures show that uncertainty in the complex refractive index brings large uncertainty in the value of the single scattering albedo; the backscat-

tering phase function in the NIR region depends significantly on the dispersion of the volume spectrum of yellow sand particles.

Volume loading of the yellow sand particles at the observation site was estimated to be 666 l/km^2 at the maximum stage of the yellow sand event and 183 l/km^2 for the secondary maximum on 8 May. Solar radiative heating of the atmosphere from 0.08 to 0.4°C/day is expected over a considerably wide area in one yellow sand event. Since large uncertainties of the volume spectrum, refractive index and backscattering phase function exist, additional measurements of the phase function and refractive index should be carried out in the future.

Acknowledgements.

Drs. R.S. Fraser and Y.J. Kaufman of Goddard Space Flight Center are gratefully acknowledged for valuable discussion.

References

Arao, K. and Y. Ishizaka, 1986: Volume and mass of yellow sand dust in the air over Japan as estimated from atmospheric turbidity. *J. Meteor. Soc. Japan*, **64**, 79–94.

Asano, S. and M. Sato, 1980: Light scattering by randomly oriented spheroidal particles. *Appl. Opt.*, **19**, 962–974.

Carlson, T.N. and S.G. Benjamin, 1980: Radiative heating rates for Saharan dust. *J. Atmos. Sci.*, **37**, 193–213.

Carlson and R.S. Caverly, 1977: Radiative characteristics of Saharan dust at solar wavelengths. *J. Geophys. Res.*, **82**, 3141–3152.

Coletti, A., 1984: Light scattering by nonspherical particles: A laboratory study. *Aerosol Sci. and Tech.*, **3**, 39–52.

Chýlek, P., G.W. Grams and R.G. Pinnick, 1977: Light scattering by nonspherical particles. *Radiation in the atmosphere*. Ed. H.-J. Bolle, Science Press, Princeton, 82–84.

Gorchakov, G.I., I.A. Gorchakova, Ye.A. Lykosov, V.G. Tolstobrov and L.S. Turovtseva, 1976: Determination of the refractive index and microstructure of foggy haze. *Izv., Atmos. Ocean. Phys.*, **12**, 371–375.

Grams, G.W., I.H. Blifford, Jr., D.A. Gillette and P.B. Russell, 1974: Complex index of refraction of airborne soil particles. *J. Appl. Meteor.*, **13**, 459–471.

Heintzenberg, J. and R.M. Welch, 1982: Retrieval of aerosol size distribution from angular scattering function: effects of particle composition and shape. *Appl. Opt.*, **21**, 822–830.

Holland, A.C. and G. Gagne, 1970: The scattering of polarized light by polydisperse systems of irregular particles. *Appl. Opt.*, **9**, 1113–1121.

Iwasaka, Y., H. Minoura, K. Nagaya and A. Ono, 1982: The transportation and spatial scale of dust storm, KOSA. - A case study on the dust storm of April 1979 measured by lidar. *Tenki*, **29**, 231–235 (in Japanese).

Kaufman, Y.J. and R.S. Fraser, 1983: Light extinction by aerosols during summer air pollution. *J. Clim. Appl. Meteor.*, **22**, 1694–1706.

Kondratyev, K.Ya, R.M. Welch, S.K. Cox, V.S. Grishechkin, V.A. Ivanov, M.A. Prokofyev, V.F. Zhvalev and O.B. Vasilyev, 1981: Determination of vertical profiles of aerosol size spectra from aircraft radiative flux measurements. 1. Retrieval of spherical particle size distribution. *J. Geophys. Res.*, **86**, 9783–9793.

Mugnai, A. and W.J. Wiscombe, 1986: Scattering from nonspherical Chebyshev particles. I: cross sections, single-scattering albedo, asymmetry factor, and backscattered fraction. *Appl. Opt.*, **25**, 1235–1244.

Nakajima, T., T. Takamura, M. Yamano, M. Shiobara, T. Yamauchi, R. Goto and K. Murai, 1986: Consistency of aerosol size distributions inferred from measurements of solar radiation and aerosols. *J. Meteor. Soc. Japan*, **64**, 765–776.

Okada, K., A. Kobayashi, Y. Iwasaka, H. Naruse, T. Tanaka and O. Nemoto, 1987: Features of individual Asian dust-storm particles collected at Nagoya, Japan. *J. Meteor. Soc. Japan*, **65**, 515–521.

Otterman, J., R.S. Fraser and O.P. Bahethi, 1982: Characterization of tropospheric desert aerosols at solar wavelengths by multispectral radiometry from Landsat. *J. Geophys. Res.*, **87**, 1270–1278.

Pinnick, R.G., D.E. Carroll and D.J. Hofmann, 1976: Polarized light scattered from monodisperse randomly oriented nonspherical aerosols: measurements. *Appl. Opt.*, **15**, 384–393.

Pollack, J.B. and J.N. Cuzzi, 1980: Scattering by nonspherical particles of size comparable to a wavelength: A new semi-empirical theory and its application to tropospheric aerosols. *J. Atmos. Sci.*, **37**, 868–881.

Schuerman, D.W., R.T. Wang, B.A.S. Gustafson and R.W. Schaefer, 1981: Systematic studies of light scattering. 1: Particle shape. *Appl. Opt.*, **20**, 4039–4050.

Shaw, G.E., 1980: Transport of Asian desert aerosol to the Hawaiian Islands. *J. Appl. Meteor.*, **19**, 1254–1259.

Shifrin, K.S. and V.A. Gashko, 1974: Determination of the microstructure of a scattering medium consisting of a mixture of particles with different indices of refraction. *Izv., Atmos. Ocean. Phys.*, **10**, 943–949.

Takamura, T. and M, Tanaka, 1978: Measurements of intensity and degree of polarization of light scattered by aerosols. *Sci. Rep. of Tohoku Univ., ser.* **5, 25**, 169–196.

Tanaka, M., T. Nakajima and T. Takamura, 1982: Simultaneous determination of complex refractive index and size distribution of airborne and water-suspended particles from light scattering measurements. *J. Meteor. Soc. Japan*, **60**, 1259–1272.

Tanaka, M., T. Nakajima, M. Shiobara, M. Yamano, T. Takamura and K. Arao, 1987: Optical proper-

ties of the turbid atmosphere in the yellow sand event over Japan. *Atmospheric Radiation, Progress and Prospects. Proceedings of the Beijing International Radiation Symposium.*, Eds. K.-N. Liou and Z. Xiuji, 596–601, Science Press.

Tanaka, M., M. Shiobara, T. Nakajima, M. Yamano and K. Arao, 1989: Aerosol optical characteristics in the yellow sand events observed in May, 1982 at Nagasaki - Part I Observations. Submitted to *J. Meteor. Soc. Japan.*, **67**, 267–278.

Tanaka, M., T. Takamura and T. Nakajima, 1983: Refractive index and size distribution of aerosols as estimated from light scattering measurements. *J. Clim. Appl. Meteor.*, **22**, 1254–1261.

Tomasi, C., F. Prodi and F. Tampieri, 1979: Atmospheric turbidity variations caused by layers of Sahara dust particles. *Contr. Atmos. Phys.*, **52**, 215–228.

Welch, R.M., S.K. Cox and K.Ya Kondratyev, 1981: Determination of vertical profiles of aerosol size spectra from aircraft radiative flux measurements, 2. The effect of particle non-sphericity. *J. Geophys. Res.*, **86**, 9795–9800.

Zerull, R.H., 1976: Scattering measurements of dielectric and absorbing nonspherical particles. *Contr. Atmos. Phys.*, **49**, 168–188.

長崎における1982年5月の黄砂の光学特性

第2部 モデル

中島映至・田中正之・山野牧[1]・塩原匡貴[2]

（東北大学理学部超高層物理学研究施設）

荒生公雄

（長崎大学教育学部地学教室）

中西裕治[3]

（英弘精機株式会社）

長崎において1982年4月24日から5月11日までポーラーネフロメータによる黄砂粒子の散乱位相関数の測定を行った。Pollack and Cuzziの半経験的理論によるモデルや、Mie散乱粒子に仮想的な吸収を導入したモデルは、黄砂粒子の強い非球形性を示唆した。また、ポーラーネフロメータを含む数種の測器の観測データから得られた黄砂粒子の体積スペクトルを用いて、波長別消散断面積、単一散乱アルベド、非対称因子、後方散乱関数を求めた。

観測地での黄砂粒子の体積濃度は、黄砂現象の最も強かった5月4~6日には666 l/km^2、続く5月8日には183 l/km^2と推定された。複素屈折率の虚数部として0.01および波長依存するモデル値を用いると、これらの値から計算される太陽放射加熱率は0.08~0.4° C/dayに達し、1回の黄砂到来により広い範囲にわたって大きな放射効果を及ぼすことが予想された。

[1]現在所属：川崎市多摩区長尾 2-9-10
[2]現在所属：気象研究所、茨城県つくば市長峰 1-1
[3]現在所属：スタビライザー株式会社、東京都練馬区西大泉 2-22-23